Bubble Injector Effect on the Gaslift Efficiency

S. Guet and G. Ooms
J. M. Burgers Center, Delft University of Technology, Laboratory for Aero- and Hydrodynamics, 2628 CB Delft, The Netherlands

R. V. A. Oliemans and R. F. Mudde
J. M. Burgers Center, Delft University of Technology, Kramers Laboratorium, 2628 BW Delft, The Netherlands

An experimental investigation has been made of the influence of the (initial) bubble size and bubble concentration distribution on the gaslift efficiency for a vertical air–water flow through a pipe of 72-mm dia. and 18-m height. Three significantly different bubble injectors were used. It was found that with decreasing bubble size, the liquid production increases at constant gas flow rate and, hence, the gaslift efficiency increases. Also, the initial concentration distribution can be significant, as this distribution can influence the coalescence of bubbles close to the injector. With decreasing bubble size, the transition from bubbly flow to slug flow can be postponed. This is one of the main reasons for the beneficial effect of the bubble size on gaslift efficiency. A theoretical model has been developed to predict the influence of the bubble size on the gaslift efficiency. The agreement is reasonable.

Introduction

In the oil industry the gaslift technique is often applied. This gravity-driven pumping technique enhances oil production by injecting gas in the production pipe and, in this way, lowering the bottom-hole pressure to enable more inflow of oil into the well bore. In practice, the diameter of the production pipe is of the order of 60 to 90 mm. The Reynolds number of the oil flow is (at conditions where gaslift is considered) rather low ($Re_l \approx 10{,}000$). The gas is injected from valves attached to the pipe wall. Large bubbles are generated with a nonsymmetric initial radial distribution. This article reports about a study on the possibility of improving the efficiency of the gaslift technique by injecting small bubbles. Previous laboratory experiments (Van Geest et al., 2001) with water and air already indicated that the gaslift efficiency can be improved by injecting small bubbles via a special inlet device consisting of a porous material. As compared to the standard gas injection via large nozzles, as used in practice, the liquid (water) production was remarkably higher.

The size of the generated bubbles influences the gaslift technique in several ways. First, small bubbles have a lower rise velocity in the liquid than large ones. Hence, the average gas concentration in the production pipe is for small bubbles higher than for large bubbles (at the same gas-injection rate). This means that the average density of the mixture is lower and the liquid production larger. A second effect is that the bubble size is known to have a drastic influence on the evolution of the radial gas fraction distribution (Serizawa et al., 1975; Liu, 1993). Small bubbles in an upward flow move toward the pipe wall, whereas large bubbles move to the center of the pipe. This is related to the interaction between the wake of the bubbles and the velocity distribution of the liquid (Tomiyama et al., 2002). For this reason the small bubbles are more evenly distributed over the cross section of the pipe (compared to large bubbles), and, therefore, the average gas concentration is (again) larger. Third, the size of the bubbles is observed to influence the transition from bubbly flow to slug flow (Van Geest et al., 2001). Bubbly flow is still possible with small bubbles at relative large values of the average gas fraction, where for the case of large bubbles slug flow would be present. The relatively large slug bubbles have a high rise velocity (compared to the small bubbles) and cause a relatively low average gas concentration in the pipe, and, thus, lower liquid production.

The objective of this article is to report about an experimental investigation carried out to study in more detail the effect of bubble size on the gaslift technique. In addition to

Correspondence concerning this article should be addressed to S. Guet.

the gaslift efficiency special attention will be paid to the influence of bubble size on the average gas concentration, on the transition from bubbly flow to slug flow, and on the radial gas concentration distribution. We used an 18-m high vertical pipe with a diameter of 72 mm. The liquid was water and the injected gas was air. Also some experimental results are reported where a surfactant is added to the water in order to reduce the surface tension and, in this way, make a more realistic simulation of practical conditions. Three different injectors were used to generate bubbles of different sizes and different initial radial concentration distribution. Single- and four-point optical-fiber probes were used to measure the void fraction, bubble sizes, and velocities.

In the following section, we discuss first an empirical relation for the transition from bubbly flow to slug flow. This relation plays an important role in the interpretation of the measurement results. In the third section, we present the experimental setup with its instrumentation. In the fourth section, the results about the influence of the three different inlet conditions (different initial bubble size and different initial radial bubble concentration distribution) on the gaslift efficiency, the flow pattern transition, and the radial bubble concentration distribution are discussed. In the fifth section, a bubble-size and flow-pattern-dependent theoretical model for the gaslift efficiency is introduced and compared with experimental data.

Flow Pattern Characterization

Low-liquid-input bubbly flow to finely dispersed bubbly flow

Bubbly pipe flows can be separated into two subregimes (Taitel et al., 1980; Chen et al., 1997): low-liquid-input bubbly flow, for which bubble breakup due to pipe flow turbulence is absent, and high-liquid-input bubbly flow (also called finely dispersed bubbly flow), for which the turbulence intensity determines the maximum bubble size (Levich, 1962; Hinze, 1975). By equating the total turbulent kinetic energy of the liquid phase to the total surface free energy of the dispersed phase, Chen et al. (1997) proposed a model for the transition from low-liquid-input bubbly flow to finely dispersed bubbly flow. It was compared with experiments performed on pipes of 25-mm to 127-mm dia. The result of this model is plotted in Figure 1 for a water–air flow and a pipe diameter $D_p = 72$ mm, as used in our experiments. The range of our liquid flow conditions is also plotted. It is clear, that for our experiments bubble breakup due to pipe flow turbulence is absent. Therefore, the size of the bubbles will mainly be dependent on the injector outlet conditions and their associated mixing regions.

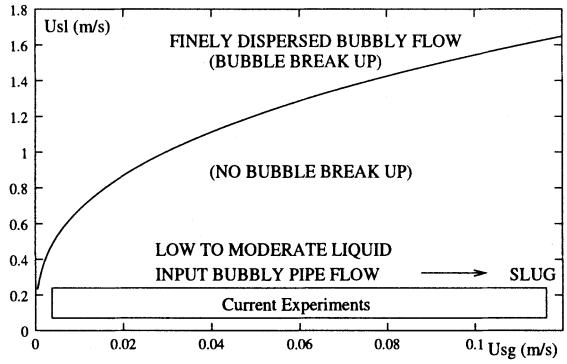

Figure 1. Boundary between low-liquid-input bubbly flow and finely dispersed bubbly flow for an air–water system of 72-mm dia. according to Chen et al. (1997): the bubbly-flow to slug-flow transition occurs in the right part.

Bubbly flow to slug flow transition

Taitel et al. (1980) assumed that the transition from bubbly flow to slug flow occurs when the gas velocity is equal to the rise velocity of large bubbles moving with respect to the averaged liquid velocity and when the void fraction has a certain critical value. Harmathy (1960) proposed the following expression for the rise velocity

$$U_{gl} = 1.53\left(\frac{g(\rho_l - \rho_g)\sigma}{\rho_l^2}\right)^{1/4} \tag{1}$$

where ρ_l is the liquid density, ρ_g the gas density, and σ the surface tension. Applying the assumption of Taitel et al. (1980), the following relation holds between the superficial liquid velocity, U_{sl}, and superficial gas velocity, U_{sg}, at the transition from bubbly flow to slug flow

$$U_{sl} = U_{sg}\frac{1-\langle\epsilon\rangle}{\langle\epsilon\rangle} - (1-\langle\epsilon\rangle)U_{gl} \tag{2}$$

in which $\langle\epsilon\rangle$ is the cross-section averaged value of the gas fraction, and U_{gl} is given by Eq. 1. As mentioned, this transition relation only holds when the gas fraction $\langle\epsilon\rangle$ is equal to the critical gas fraction ϵ_c for flow-pattern transition. By using some geometrical considerations Taitel et al. (1980) suggested $\epsilon_c = 0.25$. Other studies proposed $\epsilon_c = 0.30$ (for example, Mishima and Ishii, 1984), while the maximum gas fraction considering packed spherical shaped bubbles in a cubic lattice is $\epsilon_c = 0.52$. In a body-centered cubic configuration, $\epsilon_c = 0.68$. A generally accepted expression for the critical gas fraction is still lacking. Song et al. (1995) found a strong dependence of the transition from bubbly flow to slug flow on the injected bubble size when carrying out experiments in a narrow pipe (25 mm dia.). An expression for the critical gas fraction, ϵ_c, as a function of the nondimensional bubble size D_b/D_p was found from an interpolation of their experiments

$$\epsilon_c(D_b/D_p) = 0.55 - 2.37\frac{D_b}{D_p} \tag{3}$$

where D_b is the bubble diameter. Cheng et al. (2002) also mentioned this effect of the bubble size on the critical gas fraction corresponding to flow pattern transition by using a 28.9-mm-diameter pipe.

For small pipe diameters the initial bubble diameter can easily be of the order of the pipe diameter if special attention is not paid to the bubble inlet geometry. In such cases, breakup of large bubbles due to turbulence is necessary for a bubbly flow to develop. According to Taitel et al. (1980) low-

liquid-input bubbly flow is only possible when the pipe diameter is above a critical value, corresponding to $D_p > 52$ mm for an atmospheric-pressure air–water flow. However, this criterion cannot be generally valid since it should be bubble-inlet dependent. For very-large-diameter pipes the flow pattern is still rather uncertain. For instance, Cheng et al. (1998) studied the flow pattern in a 150-mm-dia. pipe, and found no slug flow but a churnlike flow pattern for the conditions of slug flow in a smaller-diameter pipe. In addition, Ohnuki and Akimoto (1996) mentioned the occurrence of churnlike structures in a 200-mm-dia. pipe.

In this article we apply the correlation (Eq. 3) for an air–water flow through a 72-mm-dia. pipe; the range of bubble dia. to pipe diameter was similar to the Song et al. (1995) experiments: $0.1 < D_b/D_p < 0.2$. Our criterion for the bubbly flow to slug flow transition is given by

$$U_{sl} = U_{sg}\frac{1-\epsilon_c(D_b/D_p)}{\epsilon_c(D_b/D_p)} - \left(1-\epsilon_c(D_b/D_p)\right)U_{gl} \qquad (4)$$

where U_{gl} is given by Eq. 1, and Eq. 3 is used for $\epsilon_c(D_b/D_p)$.

Experimental Setup

Gaslift facility

An air–water test facility of height $h = 18$ m and diameter $D_p = 72$ mm was used for the experiments (Figure 2). This experimental facility could be used in two different configurations by changing the downcomer part. The same perspex pipe was used for the upward bubbly flow (on the righthand side of Figure 2). In the normal gaslift situation, the liquid flow was only originating from the difference in density between the upward bubbly flow and the returning liquid flow (in the middle of Figure 2). In the second configuration, the downcomer was equipped with a centrifugal pump and a 250-L vessel in order to be able to investigate the influence of the bubble size on the gaslift efficiency at forced liquid flow rates (on the lefthand side of Figure 2).

The liquid flow rate was measured with a magnetic flowmeter. At low liquid flow rates ($U_{sl} < 0.1$ m·s^{-1}) a Rosemount Flowtube 8732C magnetic flowmeter was used, and for moderate flow rates ($0.1 < U_{sl} < 0.4$ m·s^{-1}) an Endress+Hauser Promag50 magnetic flowmeter was applied. The gas flow rate was measured with a Brooks 5861S gas mass flowmeter, providing the volumetric gas flow rate at atmospheric pressure. The pressure was measured at 2-m intervals along the pipe with pressure transducers flush mounted to the wall (AE sensors, type ATM). A remote operator controller (ROC) was used with a 100-MHz PC for sending and receiving information from the setup. The ROC could also be used to control the gas mass flow rate by means of an active valve situated upstream from the flowmeter. The bubble size and shape were first determined from photos. Since it was essential to reduce light reflections, the well-known technique of applying a square box around the pipe was used. The radial distribution of gas fraction was measured with single-optical-fiber probes at three locations downstream from the inlet: $h = 4$, 8, and 12 m, that is, $h/D_p = 55$, 110, and 166. A four-point optical probe was used to measure the individual velocity and vertical chord length of the bubbles. The four-point probe was positioned at $h = 5$ m, that is, $h/D_p = 70$.

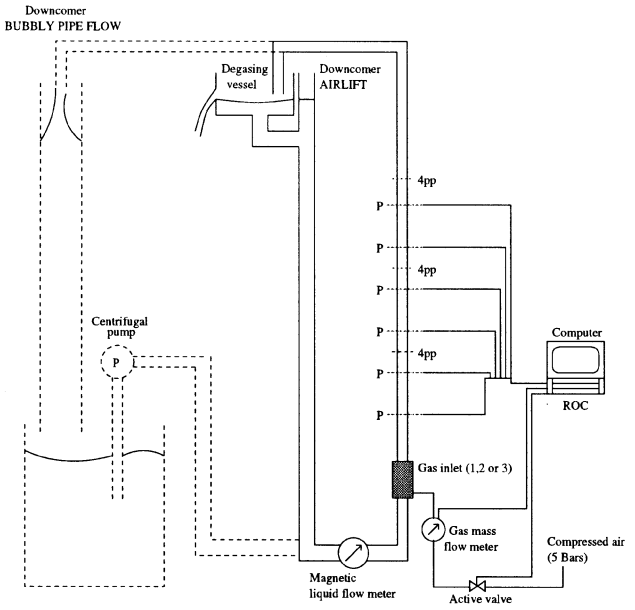

Figure 2. Experimental setup: upward bubbly pipe flow (right); downcomer for the normal airlift experiments (middle); and downcomer equipped with a centrifugal pump for airlift experiments with additional forced liquid flow (left) (the height is $h = 18$ m and the diameter $D_p = 72$ mm).

This axial position ensured measurements above the mixing zone of the bubbly flow (Liu, 1993). Due to bubble expansion, the transition from bubbly flow to slug flow always started at the top, where both the gas fraction and the bubble size were the largest.

Bubble inlets

Three different inlet devices were tested (Figure 3):

- An annular porous inlet generating small bubbles with a diameter between 1 and 8 mm. The bubbles are generated symmetrically from a horizontal circular plate.
- A long porous vertical inlet of 1 cm × 10 cm parallel to the pipe wall that also generates small bubbles with a diameter between 1 and 10 mm. The distance separating the porous plate from the pipe wall is 15 mm. The bubbles are generated perpendicularly to the liquid flow direction.
- A large-nozzle inlet, made of two 3-mm-diameter nozzle inlets attached to the pipe wall generating large bubbles with a diameter between 5 and 20 mm.

Figure 4 shows photos of the bubble distribution in the mixing region of the three bubble inlets. To achieve the same initial bubble size from the annular porous inlet and the long porous inlet, the same porous material was used (Mott Metallurgical Corp., thickness 3 mm). The pore diameter was 10 μm and the area was 1,000 mm^2 ± 50 mm^2 for the two porous medium inlets.

Four-point optical probes

Placing a glass-fiber probe in a bubbly flow allows for the local discrimination between gas (air) and liquid (water), since

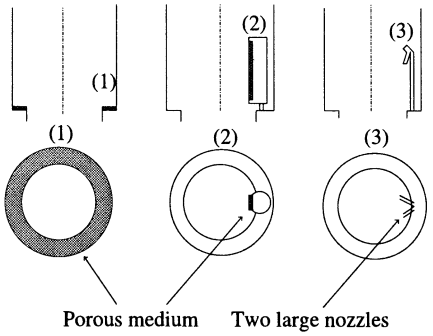

Figure 3. Top and side views of the three inlets: (1) annular porous medium inlet; (2) long porous medium inlet; and (3) large nozzle inlet.

the refractive index of air differs from the one of water, or similarly from the one of glass (Mudde and Saito, 2001). For our investigation, a four-point probe, as sketched in Figure 5, was used for the measurement of the vertical bubble velocity and vertical chord length of the bubbles. The individual bubble velocity was determined by using the mean bubble time of flight between the central fiber tip 4, situated upstream (see Figure 5) and the three other fiber tips (1, 2, 3) situated downstream. Each fiber diameter was 200 μm and the vertical distance between tip 4 and the plane (1, 2, 3) was $\Delta s = 1.6$ mm. For more information about the technique, the reader is referred to Fortunati et al. (2002) and Mudde and Saito (2001). This approach has proven to give meaningful measurements for bubbles of diameter $D_b > \Delta s$ (Fortunati et al., 2002).

Results

Inlet characterization

In order to characterize the three inlet devices, the mean vertical chord length of the bubbles was measured with the four-point probe for each inlet device at $h = 5$ m (that is, $h/D_p = 70$). For this characterization the liquid flow was kept

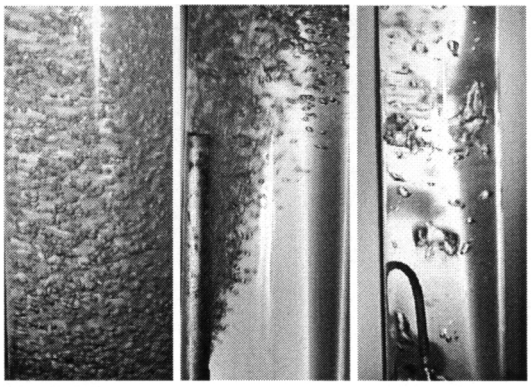

(a) Annular porous inlet (b) Long porous inlet (c) Large nozzle inlet

Figure 4. Bubble distribution in the mixing zone of the three inlets.

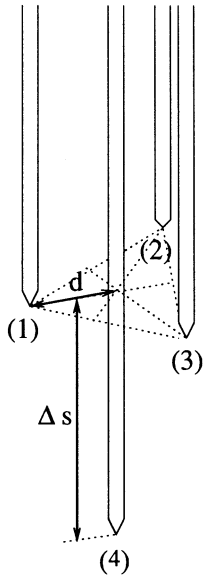

Figure 5. Perspective view of the four-point probe used.

constant at $U_{sl} = 8.2$ cm/s, and the superficial gas velocity was increased from 1 cm/s to the gas input needed for observing bubbly flow to slug flow transition (up to 9 cm/s for the annular porous inlet). Since the largest bubbles are known to be in the core region of the pipe (Liu, 1993; Lucas et al., 2001), the center line value of the bubble diameter was used for the inlet characterization. The four-point probe signal analysis, explained in Fortunati et al. (2002), was applied. Averaging was carried out over at least 500 selected bubbles, that is, measurement times of 5 to 10 min. For high void fraction ($\epsilon > 0.1$) the typical frequency of selected bubbles was 3 to 10 bubbles/s, leading to more than 1,000 selected bubbles per experimental point. The results are given in Figure 6, showing that the mean vertical chord length resulting from the two porous inlets at a low gas flow rate are nearly equal, ranging from 2.4 mm to 3.7 mm. This confirms that the porous material areas are similar (Koide et al., 1968). In contrast to the porous inlets, the large nozzle inlet was creating much larger bubbles (Figure 6). The mean vertical chord length was in that case on the order of 8.5 mm to 11 mm.

The probability density functions (PDF) for the bubble size were similar for the two porous inlets when the superficial gas velocity was low (Figure 7), that is, for low gas concentration near the inlets. When the gas flow rate was increased, coalescence occurred for the long porous inlet in the vicinity of the porous material (where the gas concentration was high), resulting in a somewhat wider distribution of the vertical chord length (Figure 7c) and a shift to the right of the density distribution. The PDF of the vertical chord length for the large nozzle showed a much wider distribution than for the porous inlets. Two peaks appeared (Figure 8), due to the presence of two groups of bubbles, namely, ellipsoidal bubbles with a typical vertical chord length between 1 and 10 mm and spherical cap bubbles with a larger vertical size.

Normal gaslift experiments

Gaslift Efficiency and Bubbly Flow to Slug Flow Transition. No additional liquid pumping was applied under normal

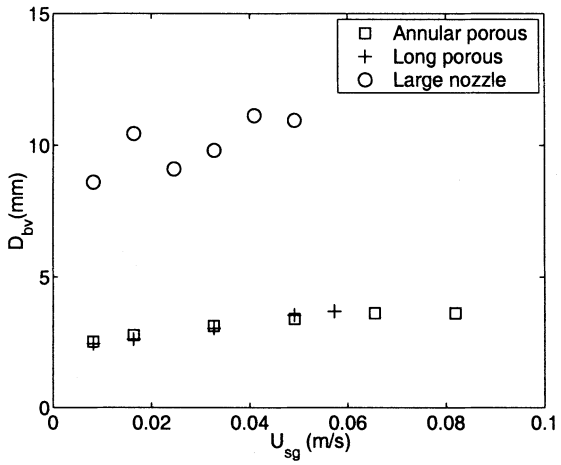

Figure 6. Mean bubble vertical chord length at $U_{sl} = 8.2$ cm/s measured at $h/D_p = 70$ on the pipe center line and using the three different inlets: the largest gas superficial velocity points for each injector are close to the transition to slug flow.

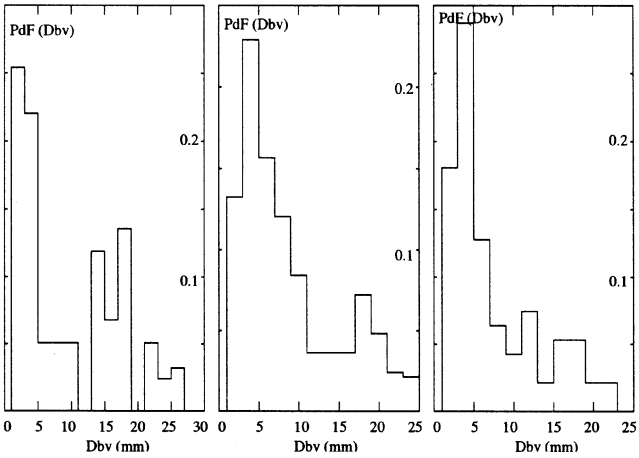

(a) $U_{sg} = 1.65cm/s$ (b) $U_{sg} = 3.3cm/s$ (c) $U_{sg} = 4.9cm/s$

Figure 8. PDF of bubble vertical chord length for the large nozzle inlet, measured at $h/D_p = 70$ at the pipe center line: the superficial gas velocity increases from (a) to (c); the flow-pattern transition is approached in (c).

gaslift conditions. The liquid flow was only due to the gas injection. The gas flow rate was increased by small steps, and the axial pressure drops and recirculating liquid flow (after reaching equilibrium) were measured. The gaslift efficiency can be evaluated in two ways. First, the generated liquid flow for a given gas flow is a measure of the efficiency of the technique. The second measure is the ratio of the pressure drop over the gaslift pipe for a certain value of the generated liquid flow, ΔP_m, and the pressure drop over the pipe for the same liquid flow and without gas injection, ΔP_l [we call this ratio $(\Delta P_m/\Delta P_l)$ the normalized pressure drop]. In Figure 9 the normalized pressure drop between $h = 2$ m and $h = 18$ m is presented for each of the three bubble injectors when operating in bubbly flow. It is evident that the annular porous inlet is the most efficient in reducing the hydrostatic pressure drop.

In Figure 10 the superficial liquid velocity generated by the injected gas flow is presented in a U_{sg} vs. U_{sl} plot, where the superficial gas velocity is given at atmospheric pressure. The observed transition points from bubbly flow to slug flow coincide with the local change of slope on the curves for the porous inlets. These local changes of slope are due to a de-

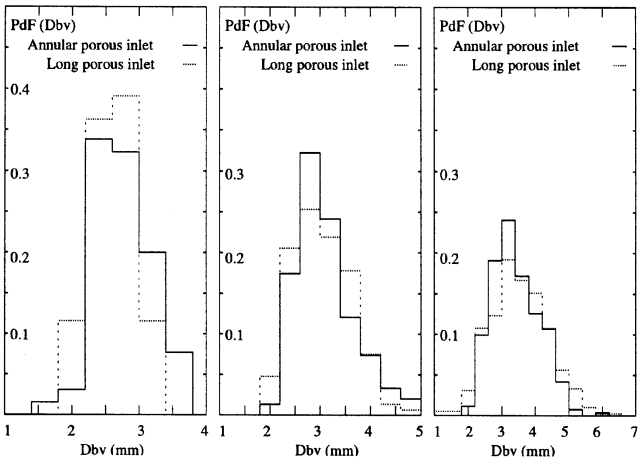

(a) $U_{sg} = 1.65cm/s$ (b) $U_{sg} = 3.3cm/s$ (c) $U_{sg} = 4.9cm/s$

Figure 7. PDF of bubble vertical chord length for the porous medium inlets, measured at $h/D_p = 70$ at the pipe center line: the superficial gas velocity increases from (a) to (c).

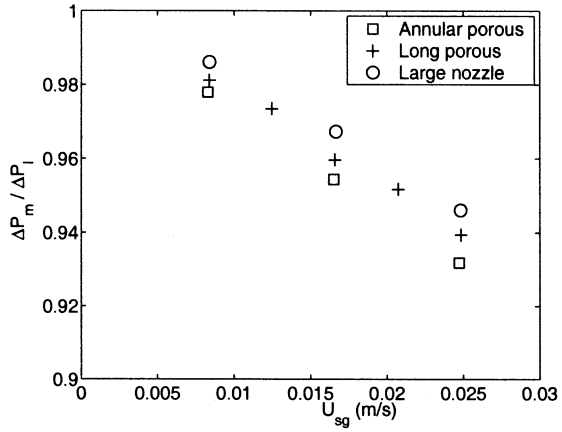

Figure 9. Normalized pressure drop for bubbly flow conditions as a function of the superficial gas velocity for the three different bubble injectors.

Due to the difference in slip velocity and void fraction distribution, the annular porous inlet is the most efficient in reducing the pressure drop.

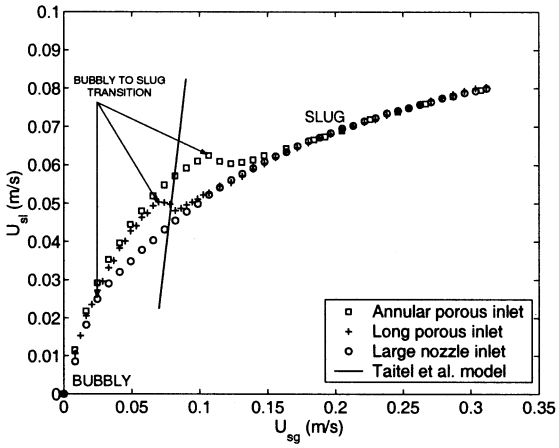

Figure 10. Liquid flow as a function of the injected gas flow for the normal airlift case and using the three different inlets; the Taitel et al. (1980) criterion for flow pattern transition is also plotted.

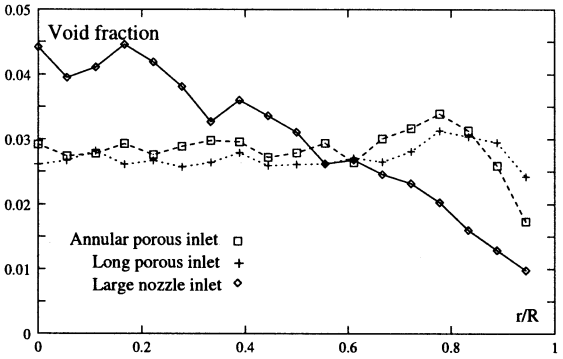

Figure 11. Radial void fraction profile measured at $h/D_p = 110$, $U_{sg} = 0.016$ ms^{-1} (that is, far from the transition boundary), and using the three bubble inlets.

crease in the gas concentration in the tube when the first slug bubbles are observed, since slug bubbles are having a significantly larger rise velocity than millimeter-size bubbles. For the large nozzle inlet, the transition occurs at much lower gas and liquid flow rates (that is, at the third point on the left of the curve). The Taitel et al. (1980) criterion for the bubbly flow to slug flow transition (with $\epsilon_c = 0.25$) is also plotted in the figure. This illustrates that this criterion cannot be generally valid. It is clear from Figure 10 that the liquid flow rate generated by the injected gas flow and also the points of transition from bubbly flow to slug flow are strongly affected by the type of bubble injector. A significant difference between the porous inlets (generating small bubbles) and the large-nozzle inlet (generating large bubbles) can be observed, even when both types of inlets are in the bubbly flow regime. Small bubbles are more efficient than large bubbles in generating a liquid flow, since they lead to higher gas fractions in the pipe due to their lower rise velocity and their ability to postpone the transition from bubbly flow to slug flow to larger values of the gas concentration.

Gas-Fraction Profiles. The gas-fraction profiles measured under airlift conditions at $h = 8$ m for the three different bubble injectors are presented in Figure 11. For small bubbles at low gas flow rate conditions (far away from the bubbly flow to slug flow transition boundary) the profiles are flat with a wall peaking profile (see the curves for the porous inlets in Figure 11). However, when injecting large bubbles, the profiles are core peaking (see the curve for the large-nozzle inlet in Figure 11). During the experiments it was observed that the transition from bubbly flow to slug flow always starts from flow conditions with a core peaking profile. The airlift efficiency was found to be better when operating at wall peaking conditions than at core peaking conditions (Figures 9, 10, and 11).

The gas-fraction profiles corresponding to the two porous inlets at low gas flow rate conditions are similar at $h/D_p = 110$, showing that the initial distribution of the bubbles is not relevant in itself for the downstream development of the radial gas-fraction profile at low void fraction. This also proves that the wall peaking behavior is not an entrance effect. However, the transition from wall peaking to core peaking was occurring at a lower gas fraction for the long porous inlet than for the annular porous inlet. This was due to some quick bubble coalescence near to the porous surface of the long porous inlet.

Due to the decrease in pressure with height, the bubbles grow in size with height in the pipe. Since larger bubbles have a tendency to move to the pipe center, it can be expected that the bubble distribution goes from wall peaking to core peaking. Figures 12 and 13 indeed show (for the annular porous inlet) the evolution from wall peaking to core peaking with height at $U_{sg} = 0.016$ ms^{-1} and $U_{sg} = 0.04$ ms^{-1}. The core peaking radial profile was rapidly reached (at $h/D_p = 160$ in Figure 13), probably due to the interaction between the wake of the bubbles and the shear in the liquid flow (Tomiyama et al., 2002).

Experiments with Surface-Active Agent. Adding a surface-active agent to the liquid reduces the size of the generated bubbles (Koide et al., 1968) and limits coalescence. For the case of the annular porous inlet, experiments with 0.5% vol-

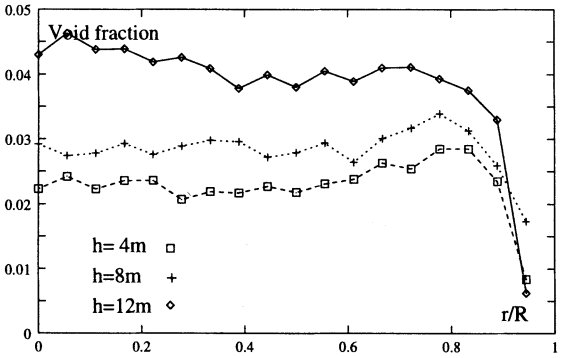

Figure 12. Radial void fraction profile evolution with height measured at $h/D_p = 56$, 110 and 166, $U_{sg} = 0.016$ ms^{-1}, and using the annular porous inlet; the profile remains wall peaking to flat with height.

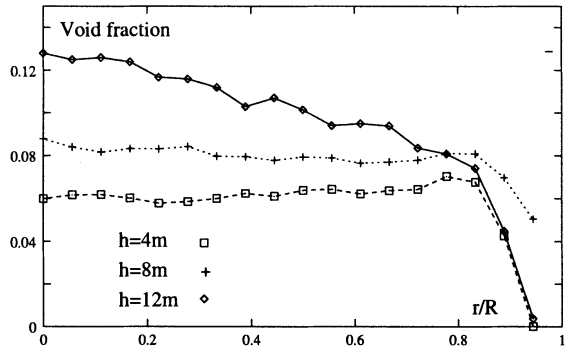

Figure 13. Radial void fraction profile evolution with height measured at $h/D_p = 56$, 110 and 166, $U_{sg} = 0.04$ ms^{-1}, and using the annular porous inlet.

The profile evolves from wall peaking to core peaking with height. At this particular gas flow value, the bubble diameter is $D_b \approx 5.5$ mm.

ume ethanol in water indeed showed that the bubble diameter was much smaller ($D_b \approx 1$–2 mm according to photos for the water–ethanol solution, compared to $D_b \approx 2$–8 mm for water). The wall peaking profile was kept for much larger height to diameter ratios. The associated airlift production curve in bubbly flow showed a remarkable improvement as compared to the water results (Figure 14).

Gaslift experiments at forced liquid flow

Bubbly Flow to Slug Flow Transition. A centrifugal pump was used in the experimental setup shown in Figure 2 in order to be able to make measurements at forced liquid flow rates. Particular attention was given to the measurement of the transition from bubbly flow to slug flow at various pump conditions. For a certain pump condition the gas flow rate was increased by small steps, starting with the bubbly flow and leading to the transition to slug flow. The flow pattern transition was determined from the pressure signal, since it became strongly nonstationary under conditions of slug flow. This was also confirmed by visual observation. Moreover, the liquid flow rate development under increasing gas flow rate conditions (at a certain pump condition) confirmed the presence of slug flow. Figure 15 presents all the measured transition points obtained with the three inlets. As expected, the transition points are again strongly dependent on the type of bubble injector. The figure also contains a comparison with model predictions from Eq. 4. The best fit was found when choosing $D_b = 7$ mm (for the annular porous inlet) and 13 mm (for the large-nozzle inlet). As mentioned, this model involves the use of the relation of Song et al. (1995) for the critical void fraction in the Taitel et al. (1980) criterion, combined with the Harmathy (1960) expression.

It is interesting to compare the bubble diameters chosen to give the best fit in Figure 15 with the bubble diameters actually measured. The mean bubble size D_b of the ellipsoidal bubbles generated by the inlets were evaluated from the measurements of the vertical chord length, D_{bv}, and an estimate of the bubble aspect ratio, χ, by means of the following relation

$$D_b = D_{bv}\chi^{2/3} \tag{5}$$

For both the long and annular porous inlets the bubble vertical chord length was 3.6 mm near the transition (Figure 6). The aspect ratio was determined by making use of photos, leading to $\chi = 2.5$ and $D_b = 7$ mm for the porous inlets. This is in agreement with the chosen value for the bubble diameter of the annular porous inlet.

The transition points for the long porous inlet are shifted to the left compared to those for the annular porous inlet. This could be due to the wider distribution of the bubble size and the nonsymmetric initial concentration for the long porous inlet. This is caused by the fact that the bubbles were generated perpendicularly to the flow in the case of the long porous inlet. This resulted in an increased gas flow recirculation and a tendency of the bubbles in the plume to remain

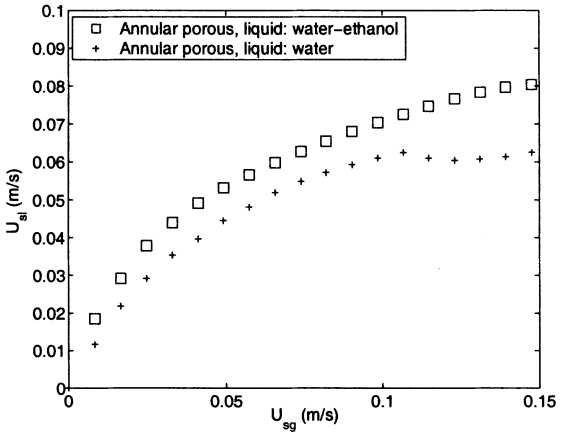

Figure 14. Liquid flow as a function of the injected gas flow from the normal airlift case, and using water and water +0.5% volume ethanol in solution; the estimated bubble diameter in the ethanol solution is $D_b \approx 1-2$ mm.

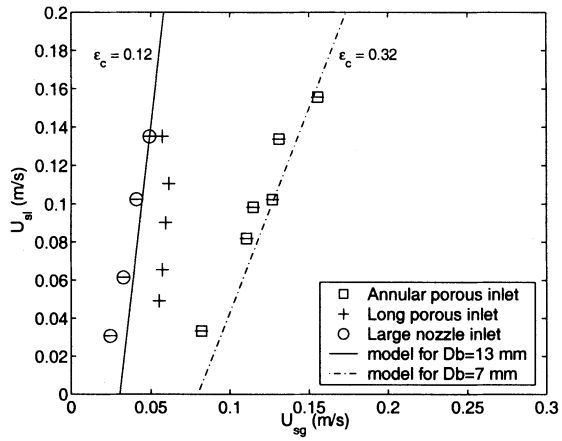

Figure 15. Bubbly flow to slug flow transition points for the three inlets; U_{sg} is given at atmospheric pressure.

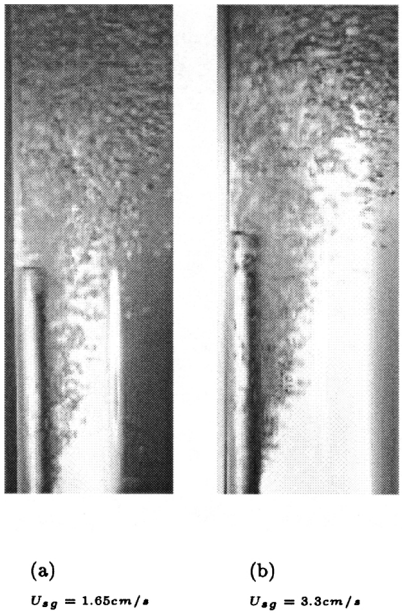

Figure 16. Bubble concentration distribution in the mixing zone of the long porous inlet for two gas flow rates.

close together when the gas and liquid flow rates were increased. Those effects are illustrated with photos of the long porous inlet mixing region for different flow conditions in Figure 16. They cause the bubbles to coalese near the long porous inlet. This coalescence (causing larger bubbles) initiated a transition to slug flow at (nearly) fixed gas flow conditions (Figure 15). Therefore, not only is the initial bubble size important, but also the initial bubble concentration distribution.

The large-nozzle inlet generated both ellipsoidal-shaped bubbles and spherical cap bubbles. If the vertical chord length was larger than 10 mm, the bubbles were treated as spherical caps (according to $E_o = (g\rho_l D_b^2/\sigma) > 40$; Tomiyama, 1998). For a smaller chord length, the bubbles were assumed to be ellipsoidal shaped. This leads to $D_b = 12.2$ mm at the transition from bubbly flow to slug flow. Again this is in reasonable agreement with the chosen value of $D_b = 13$ mm for the large-nozzle inlet.

Average Gas Fraction and Gaslift Efficiency. In the range of the low liquid flow conditions of our experiments the friction and acceleration contribution to the pressure drop is negligible. Since $\langle \epsilon \rangle \rho_g \ll (1 - \langle \epsilon \rangle)\rho_l$, the average gas fraction can be estimated from pressure-drop measurements by means of

$$\langle \epsilon \rangle = 1 - \frac{\Delta P}{\Delta h \rho_l g} \tag{6}$$

where ΔP is the pressure difference between two measurement points and Δh is the distance between these points. The contribution of the air density is neglected because of the low-pressure conditions used. We used this equation to calculate the average gas fraction from the measured pressure drop at the transition from bubbly flow to slug flow. Since this transition always started at the top of the pipe, the pressure drop was calculated by using the pressure difference between $h_1 = 12$ m and the top (that is, $h_2 = 18$ m). The average gas fraction between h_1 and h_2 associated with flow pattern transition, and calculated from the average pressure drop, was 0.3 for the annular porous inlet, which is comparable to $\epsilon_c(D_b = 7 \text{ mm}, D_p = 72 \text{ mm}) = 0.32$ calculated from the Song et al. (1995) correlation (Eq. 3). The average gas fraction for the large nozzle inlet at transition (calculated from the measured pressure drop) is 0.1, while the Song et al. correlation predicts $\epsilon_c = 0.12$. This shows that this correlation gives reliable predictions. It also confirms that the average gas fraction for bubbly flow to slug flow transition is strongly affected by the size of the injected bubbles. Moreover it proves again that the gaslift efficiency is significantly increased when using small bubbles (as a larger gas fraction means a smaller pressure drop).

A Simple Theoretical Model for the Influence of the Bubble Size on the Pressure Drop

As mentioned in the Introduction the effect of the bubble size on the gaslift efficiency can be split into the following three parts: small bubbles have a lower rise velocity than large bubbles, small bubbles postpone the transition from bubbly flow to slug flow compared to large bubbles, and small bubbles distribute more evenly over the pipe cross section than large bubbles. A simple theoretical model has been developed, based on the drift-flux model of Zuber and Findlay (1965), to predict the overall effect of the bubble size on the pressure gradient in a pipe under gaslift conditions. It is described below.

Bubble rise velocity

Bubbly Flow. According to the Harmathy expression given by Eq. 1, the bubble rise velocity, U_{gl}, is independent of the bubble diameter. However, Peebles and Garber (1953) showed that the rise velocity of a single bubble in an infinite medium is dependent on the bubble size. As we want to use our theoretical model to study the influence of the bubble diameter on the pressure drop (and, thus, on the gaslift efficiency), we will apply this expression. For an air bubble in water, it is given by:

- $U_{gl} = 1.35\left(\frac{2\sigma}{\rho_l D_b}\right)^{1/2}$ for 2.1 mm $< D_b <$ 4.1 mm,
- $U_{gl} = 1.53\left(\frac{g(\rho_l - \rho_g)\sigma}{\rho_l^2}\right)^{1/4}$ for 4.1 mm $< D_b <$ 12.4 mm,
- $U_{gl} = \left(\frac{gD_b}{2}\right)^{1/2}$ for $D_b >$ 12.4 mm.

A correction of this expression is still necessary at higher values of the bubble concentration due to the hydrodynamic interaction between the bubbles. For that reason we introduce the bubble drift velocity U_{drift} which is defined as the rise velocity of a bubble with respect to the mixture velocity of the two-phase system at a finite value of the gas concentration. We use the following expression for the drift velocity (Richardson and Zaki, 1954)

$$U_{\text{drift}} = U_{gl}(1 - \langle \epsilon \rangle) \tag{7}$$

Slug Flow. In case of slug flow, the drift velocity of a slug bubble is given by (Mishima and Ishii, 1984)

$$U_{\text{drift,slug}} = 0.35\left(\frac{g\Delta\rho D_p}{\rho_l}\right)^{1/2} \tag{8}$$

Flow pattern

As discussed, the transition from bubbly flow to slug flow only takes place when the gas fraction is larger than the critical value ϵ_c (which depends on the bubble size). In our model we apply Eq. 3 based on the work of Song et al. (1995) for the critical concentration. So we apply the following criteria:

- If $(\langle \epsilon \rangle) < \epsilon_c$, bubbly flow is assumed to be present in the pipe;
- If $(\langle \epsilon \rangle) > \epsilon_c$, slug flow is assumed to be present.

Radial gas-fraction distribution

For small (typically $D_b < 5.5$ mm) air bubbles in water the radial gas-fraction distribution is known to exhibit a peak near the wall (Serizawa et al., 1975; Liu, 1993). Larger bubbles led to a parabolic type of profile. Tomiyama et al. (2002) have shown that there is a critical *Eo* number above which bubbles move from the wall to the center region of the pipe. A related transverse lift force coefficient as a function of the bubble diameter was deduced from single-bubble experiments in a simple shear flow. The result is shown in Figure 17 for air bubbles in water. Lucas et al. (2001) successfully applied this approach in a two-fluid model to describe wall peaking and core peaking profiles.

According to Rivière and Cartellier (1999), the wall peaking void fraction profile can be described by means of three zones, in each of which the gas fraction has a certain constant value. In between a wall peaking and core peaking profile the radial gas fraction profile can be described by $\epsilon/\epsilon_M = (1-(r/R)^n$, in which ϵ_M is the gas fraction at the center line of the pipe. (The exponent n changes from $n = 7$ for a flat profile to $n = 2$ for a parabolic void fraction profile.)

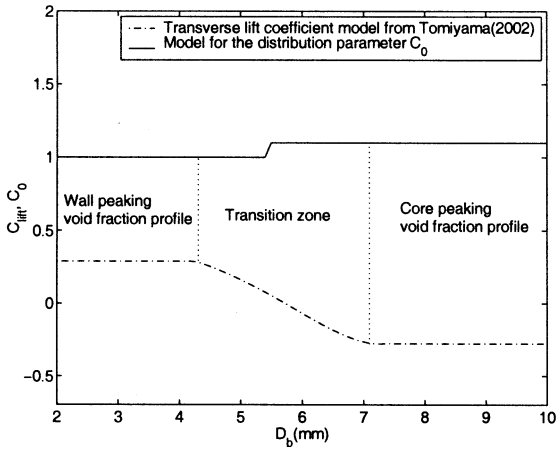

Figure 17. Lift force coefficient for an air–water bubble, and a model for the associated distribution parameter C_0.

To include the effect of the bubble diameter on the radial gas-fraction profile we apply the drift-flux model of Zuber and Findlay (1965). According to this model, the following relation holds: $\langle \epsilon \rangle = U_{sg}/\langle U_g \rangle$, with $\langle U_g \rangle = C_0(U_{sg} + U_{sl}) + \overline{U_{\text{drift}}}$, where $\langle U_g \rangle$ is the cross-section averaged value of the gas velocity and C_0 is the distribution parameter. The mean drift velocity $\overline{U_{\text{drift}}}$ is taken as the drift velocity U_{drift} described in Eqs. 7 and 8. The value of the distribution parameter depends on the radial gas-fraction profile and changes from $C_0 \approx 1$ for a wall peaking gas fraction profile to $C_0 \approx 1.1$ for a core peaking profile and $C_0 = 1.2$ for slug flow. For our model predictions for the flow of air bubbles in water we therefore choose the following values for the distribution parameter (see Figure 17):

- If $D_b < 5.5$ mm: $C_0 = 1$;
- If $D_b > 5.5$ mm: $C_0 = 1.1$;
- In case of slug flow ($(\langle \epsilon \rangle) > \epsilon_c$): $C_0 = 1.2$.

Pressure drop predictions

We computed the pressure gradient in the pipe between $h = 12$ m and $h = 18$ m for the case of our gaslift experiments by using the following bubble-diameter-dependent calculation procedure.

(1) We assume bubbly flow. From the known bubble diameter, D_b, the bubble rise velocity, U_{gl}, and the distribution parameter, C_0, are calculated by means of the expressions discussed earlier.

(2) The averaged gas fraction $\langle \epsilon \rangle$ is determined from the drift-flux model. To apply this model, the values of U_{sg} and U_{sl} are needed (see below).

(3) Using the known values of U_{sl}, U_{sg}, U_{gl}, and D_b the critical gas fraction ϵ_c can be calculated from the criterion for the bubbly flow to slug flow transition given by Eq. 4. When the averaged gas fraction is smaller than its critical value, bubbly flow is still assumed to be present. When it is larger, slug flow is present. In that case, the slug-flow expressions for the rise velocity and the distribution parameter are applied.

(4) The hydrostatic pressure gradient $(\partial P/\partial z)_H = (1 - \langle \epsilon \rangle)\rho_l g$ was computed using the value of the gas fraction.

Using the model just described, the normalized pressure drop between $h = 12$ m and $h = 18$ m (in the pipe used for our gaslift experiments) was computed for several values of the bubble diameter ($D_b = 4$ mm, 7 mm, and 13 mm) representing the bubble sizes generated by the different bubble injectors. The annular porous inlet (respectively, at low and high values of injected gas) is represented by $D_b = 4$ mm and $D_b = 7$ mm. Accordingly, the superficial liquid velocities experimentally obtained with the annular porous inlet for different values of the superficial velocity of injected gas was used in step 2 of the calculation procedure. This superficial liquid velocity can in principle be calculated by taking the flow characteristics of the pipe loop into account. For this preliminary calculation, however, we preferred to use the experimental value. The large-nozzle inlet is represented by $D_b = 13$ mm, and the superficial liquid velocities obtained for the large-nozzle inlet were applied. The theoretical predictions are given in Figure 18 and compared with experimental data. The bends in the theoretical curves represent the transition from bubbly flow to slug flow. At low values of injected

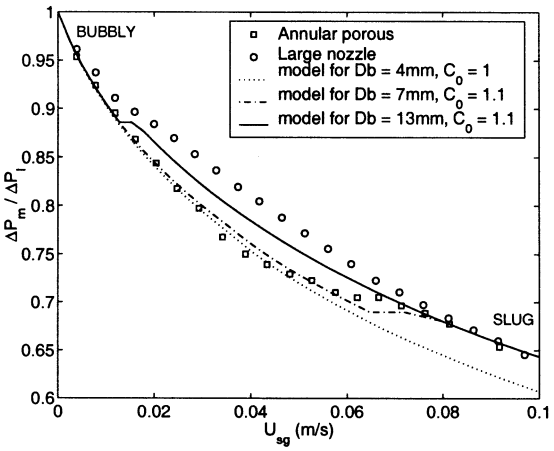

Figure 18. Comparison between the normalized pressure drop between $h = 12$ m and $h = 18$ m obtained with the theoretical model and from the experiments; U_{sg} is given at $h = 12$ m.

gas the predictions for the annular porous inlet are in good agreement with the experimental data for $D_b = 4$ mm, and at large values of injected gas, with the data for $D_b = 7$ mm. This is in agreement with expectation, as the bubble size generated by the porous material increases with superficial gas velocity (see Figure 6). The transition from bubbly flow to slug flow is correctly predicted when using $D_b = 7$ mm. With $D_b = 4$ mm this transition is postponed to unrealistically high values of the superficial gas velocity. The predictions for the large-nozzle inlet correctly show the negative effect of larger bubbles on the gaslift efficiency, although the quantitative agreement between the predictions and experimental data is less good than for the annular porous inlet.

Conclusion

The influence of three different bubble injectors on the gaslift efficiency was investigated experimentally in a vertical pipe of 72-mm dia. and 18-m height. Three different bubble injectors were used that had a significant influence on the initial bubble size and on the initial radial gas fraction profile. The evolution of the gas fraction profile from wall peaking to core peaking, and the transition from bubbly flow to slug flow was monitored as a function of the gas flow rate and bubble size for the three injectors. The efficiency of the airlift technique was shown to be strongly dependent on the type of bubble injector. Small bubbles caused the largest gaslift efficiency, as small bubbles have a low rise velocity and a more evenly distributed gas concentration in a pipe cross section.

Moreover with small bubbles the transition from bubbly flow to slug flow is postponed to larger values of injected gas. The average gas fraction associated with the flow pattern transition changed from 10% to 30% when the bubble diameter was reduced from 13 mm to 7 mm. The flow pattern transition for the three injectors used in our 72-mm dia. air–water experiments could be predicted properly by using the expression for the critical void fraction based on the experiments of Song et al. (1995) for a 25-mm dia. air–water pipe flow. However, the geometry of the bubble generation device was also found to affect the gaslift efficiency. A difference between the annular porous inlet and the long vertical porous inlet could be observed. This was due to bubble coalescence in the case of the long porous inlet close to the injector, in particular at larger values of the gas and liquid flow rate. So not only the type of injector material is important, but also the geometry of the injector surface.

Based on the drift-flux model, a simple theoretical model has been developed to account for the bubble size effect on the bubble rise velocity, the radial gas fraction distribution, and the transition from bubbly flow to slug flow. The predictions are in reasonable agreement with experiments. An interesting subject of further research would be to investigate in more detail how the void fraction and phase velocities are coupled in upward bubbly pipe flows, and how the drift-flux parameters are affected by the void fraction and velocity conditions.

Acknowledgments

Financial support was provided by the European Community (project "Non Ideal Turbulence"). The experimental setup was provided by Shell EP, Rijwijk, The Netherlands. We acknowledge Ir. S. Van Geest for his work on the airlift experimental setup and Dr. J. H. Ellepola for initiating this investigation.

Literature Cited

Chen, X. T., X. D. Cai, and J. P. Brill, "A General Model for Transition to Dispersed Bubble Flow," *Chem. Eng. Sci.*, **52**, 4373 (1997).

Cheng, H., J. H. Hills, and B. J. Azzorpardi, "A Study of the Bubble-to-Slug Transition in Vertical Gas-Liquid Flow in Columns of Different Diameter," *Int. J. Multiphase Flow*, **24**, 431 (1998).

Cheng, H., J. H. Hills, and B. J. Azzorpardi, "Effect of Initial Bubble Size on Flow Pattern Transition in a 28.9 mm Diameter Column," *Int. J. Multiphase Flow*, **28**, 1047 (2002).

Fortunati, R. V., S. Guet, G. Ooms, R. V. A. Oliemans, and R. F. Mudde, "Accuracy and Feasibility of Bubble Dynamic Measurements with Four-Point Optical Fiber Probes," Symposium on the Application of Laser Techniques to Fluid Mechanics, Lisbon, Portugal (2002).

Harmathy, T. Z., "Velocity of Large Drops and Bubbles in Media of Infinite or Restricted Extent," *AIChE J.*, **6**, 281 (1960).

Hinze, J. O., *Turbulence*, McGraw-Hill, New York (1959).

Koide, K., S. Kato, Y. Tanaka, and H. Kubota, "Bubble Generated from Porous Plate," *J. Chem. Eng. Jpn.*, **5**, 51 (1968).

Levich, V. G., *Physicochemical Hydrodynamics*, Prentice Hall, Englewood Cliffs, NJ (1962).

Liu, T. J., "Bubble Size and Entrance Length Effect on Void Development in a Vertical Channel," *Int. J. Multiphase Flow*, **19**, 99 (1993).

Lucas, D., E. Krepper, and H. M. Prasser, "Prediction of Radial Gas Profiles in Vertical Pipe Flow on the Basis of Bubble Size Distribution," *Int. J. Therm. Sci.*, **40**, 217 (2001).

Mishima, K., and M. Ishii, "Flow Regime Transition Criteria for Upward Two-Phase Flow in Vertical Tubes," *Int. J. Heat Mass Transfer*, **27**, 773 (1984).

Mudde, R. F., and T. Saito, "Hydrodynamical Similarities Between Bubble Column and Bubbly Pipe Flow," *J. Fluid Mech.*, **437**, 203 (2001).

Ohnuki, A., and H. Akimoto, "An Experimental Study on Developing Air-Water Two Phase Flow Along a Large Diameter Pipe: Effect of Air Injection Method," *Int. J. Multiphase Flow*, **22**, 1143 (1996).

Peebles, F. N., and H. J. Garber, "Studies on the Motion of Gas Bubbles in Liquids," *Chem. Eng. Prog.*, **49**, 88 (1953).

Richardson, J. F., and W. N. Zaki, "Sedimentation and Fluidization: Part 1," *Trans. Inst. Chem. Eng.*, **32**, 35 (1954).

Rivière, N., and A. Cartellier, "Wall Shear Stress and Void Fraction in Poiseuille Bubbly Flows: Part 1: Simple Analytic Predictions," *Eur. J. Mech. B/Fluids*, **18**, 823 (1999).
Serizawa, A., I. Kataoka, and I. Michiyoshi, "Turbulence Structure of Air-Water Bubbly Flows—2. Local Properties," *Int. J. Multiphase Flow*, **2**, 235 (1975).
Song, C. H., H. C. No, and M. K. Chung, "Investigation of Bubble Flow Developments and Its Transition Based on the Instability of Void Fraction Waves," *Int. J. Multiphase Flow*, **21**, 381 (1995).
Taitel, Y., D. Barnea, and A. E. Dukler, "Modelling Flow Pattern Transitions for Steady Upward Gas-Liquid Flow in Vertical Tubes," *AIChE J.*, **26**, 345 (1980).
Tomiyama, A., "Struggle with Computational Bubble Dynamics," *Int. Conf. on Multiphase Flow*, ICMF '98, Lyon, France (1998).
Tomiyama, A., H. Tamai, I. Zun, and S. Hosokawa, "Transverse Migration of Single Bubbles in Simple Shear Flow," *Chem. Eng. Sci.*, **57**, 1849 (2002).
Van Geest, S., J. H. Ellepola, and R. V. A. Oliemans, "Comparison of Different Air Injection Methods to Improve Gas-Lift Performance," *Proc. Conf. Multiphase 01*, Cannes, France, p. 363 (2001).
Zuber, N., and J. A. Findlay, "Average Volumetric Concentration in Two-Phase Flow Systems," *J. Heat Transfer Trans. ASME*, **87**, 453 (1965).

Manuscript received Sept. 9, 2002, and revision received Mar. 3, 2003.